

Umbrianite, $K_7Na_2Ca_2[Al_3Si_{10}O_{29}]F_2Cl_2$, a new mineral species from melilitolite of the Pian di Celle volcano, Umbria, Italy

VICTOR V. SHARYGIN^{1,*}, IGOR V. PEKOV², NATALIA V. ZUBKOVA², ALEXANDER P. KHOMYAKOV^{3†},
FRANCESCO STOPPA⁴ and DMITRY YU. PUSHCHAROVSKY²

¹ V.S. Sobolev Institute of Geology and Mineralogy, Siberian Branch of the RAS, 3 prosp. Akad. Koptyuga, Novosibirsk 630090, Russia

*Corresponding author, e-mail: sharygin@igm.nsc.ru

² Faculty of Geology, Moscow State University, Vorobievsky Gory, Moscow 119991, Russia

³ Institute of Mineralogy, Geochemistry and Crystal Chemistry of Rare Elements, Veresaev Street 15, Moscow 121357, Russia

⁴ Dipartimento di Scienze della Terra, Gabriele d'Annunzio University, Campus Madonna delle Piane, Chieti 66013, Italy

Abstract: The new mineral umbrianite, ideally $K_7Na_2Ca_2[Al_3Si_{10}O_{29}]F_2Cl_2$, was discovered as an essential groundmass mineral in melilitolite of the Pian di Celle volcano, Umbria, Italy. It forms rectangular, lamellar or lath-shaped crystals (up to $25 \times 30 \times 200 \mu\text{m}$), typically flattened on {010}, and sheaf-like aggregates (up to 200–500 μm across). Umbrianite is commonly associated with kalsilite, leucite, fluorophlogopite, melilite, olivine ($Fo_{>60}$), diopside, nepheline, Ti-rich magnetite, fluorapatite, cuspidine–hiortdahlite series minerals, götzenite, khibinskite, monticellite–kirschsteinite series minerals, westerveldite, various sulphides and peralkaline silicate glass. The empirical formula (based on $Si + Al + Fe^{3+} = 13$) of the holotype umbrianite (mean of 58 analyses) is $(K_{6.45}Na_{0.35}(Sr,Ba)_{0.01})_{\Sigma 6.81}(Na_{1.22}Ca_{0.78})_{\Sigma 2.00}(Ca_{1.85}Mg_{0.13}Mn_{0.01}Ti_{0.01})_{\Sigma 2.00}[(Fe^{3+}_{0.34}Al_{3.06}Si_{9.60})_{\Sigma 13.00}O_{29.00}]F_{2.05}Cl_{1.91}(OH)_{0.04}$. The strongest lines of the X-ray diffraction powder pattern $\{d[\text{Å}] (I_{\text{obs}})\}$ are: 9.65(100), 6.59(97), 3.296(77), 3.118(70), 2.819(53), 2.903(52), 6.91(43). The strong bands in the Raman spectrum of umbrianite are at 525, 593, 735 and 1036 cm^{-1} . The mineral is orthorhombic, space group $Pmnm$, unit-cell parameters are: $a = 7.0618(5)$, $b = 38.420(2)$, $c = 6.5734(4) \text{ Å}$, $V = 1783.5(2) \text{ Å}^3$, $Z = 2$. The calculated density is 2.49 g/cm^3 . The crystal structure of umbrianite has been refined from X-ray single-crystal data to $R = 0.0941$ for 1372 independent reflections with $I > 2\sigma(I)$. Umbrianite is a representative of a new structure type. Its crystal structure contains the triple-layer tetrahedral blocks $[Al_4(Si,Al)_2(Si,Al,Fe)_4Si_{16}O_{58}]^{\infty}$ connected to each other via the columns of edge-shared octahedra CaO_3F to form a 3D quasi-framework with channels filled by Cl^- , K^+ (inside the tetrahedral blocks) and Na^+ (between the Ca octahedral columns). Umbrianite, günterblässite and hillesheimite, containing topologically identical triple-layer tetrahedral blocks, form the günterblässite group. Umbrianite is unstable under postmagmatic hydrothermal conditions and alters to Ba-rich hydrated phases.

Key-words: umbrianite, new mineral, günterblässite, hillesheimite, delhayelite, phyllosilicate, crystal structure, melilitolite, kamafugite, Pian di Celle volcano, Italy.

1. Introduction

Umbrianite, $K_7Na_2Ca_2[Al_3Si_{10}O_{29}]F_2Cl_2$, was approved by the CNMNC IMA as a new mineral species in October 2011 (IMA #2011-074). The mineral is named for Umbria, the region of Central Italy where its type locality, the Pian di Celle volcano, is situated. The type specimens of umbrianite (sample number U-3a) are deposited in the collections of the Fersman Mineralogical Museum of the Russian Academy of Sciences, Moscow, Russia (registration number 4157/1), and in the Central Siberian Geological Museum at V.S. Sobolev

Institute of Geology and Mineralogy (IGM), Novosibirsk, Russia (catalogue number XIII-338/1).

Umbrianite was first described in melilitolite from the same locality as a “delhayelite-like mineral” on the basis mainly of its chemical composition (Stoppa *et al.*, 1997; Sharygin, 2002). Later, more detailed studies showed that this mineral is a representative of the new, triple-layer phyllosilicate structure type, similar to günterblässite, $(K,Ca,Ba,Na,\square)_{3-x}Fe[(Si,Al)_{13}O_{25}(OH,O)_4] \cdot 7H_2O$ (Chukanov *et al.*, 2012a; Rastsvetaeva *et al.*, 2012) and hillesheimite, $(K,Ca,Ba,\square)_2(Mg,Fe,Ca,\square)_2[(Si,Al)_{13}O_{23}(OH)_6](OH) \cdot 8H_2O$ (IMA #2011-080, Chukanov *et al.*, 2012b), which constitute the günterblässite group. Delhayelite, a

†Deceased in October 2012

mineral chemically related to umbrianite, is a double-layer silicate of the rhodesite mero-pleisotype series (Pekov *et al.*, 2009). In this paper we provide a detailed description of umbrianite.

2. Geological background for Pian di Celle

The Pian di Celle volcano is a part of a Pleistocene kamafugite-carbonatite province located along grabens in the Apennines (Fig. 1), in an area characterized by intense emissions of CO₂ and seismicity associated with normal faulting, on a continental lithosphere that is 80–110 km thick (Lavecchia & Boncio, 2000). The Pian di Celle tuff-ring and lava flow belong to the San Venanzo volcanic complex, which also comprises a large maar and a small isolated diatreme (Fig. 1). Peralkaline kamafugite and phonolitic foidite make up 80 % of the volcano's volume (Stoppa & Cundari, 1998; Zanon, 2005), in which the lava flow is a leucite–kalsilite–olivine melilitite (the local name: venanzite). The remaining 20 % of the volcano volume includes carbonatite tuffs that form indurate beds of mixed carbonatite–melilitite agglomerates and ash-fall carbonatite layers. The pegmatoid kamafugitic melilitolites represent the final event in the development of the Pian di Celle volcano (Stoppa, 1995). They form a dykelet swarm in the NE flow front of the Le Selvarelle venanzite lava of the Pian di Celle volcano, Vispi Quarry, San Venanzo volcanic area, Terni Province, Umbria, Italy (Cundari & Ferguson, 1994; Stoppa, 1995; Sharygin *et al.*, 1996a and b; Stoppa & Woolley, 1997; Stoppa

et al., 1997; Stoppa & Cundari, 1998; Panina *et al.*, 2003). Note that Pian di Celle is also the type locality for the zeolite willhendersonite (Peacor *et al.*, 1984).

3. Analytical methods

The morphological data, elemental maps and preliminary chemical data for umbrianite and associated minerals were obtained using JEOL JSM-35 and JEOL JSM6380LA scanning microscopes at the V.S. Sobolev Institute of Geology and Mineralogy (IGM) in Novosibirsk.

The chemical composition of umbrianite was studied using a “Camebax-micro” electron microprobe (IGM) at an accelerating voltage of 20 kV, probe current of 10–16 nA, and 2–5 μm beam diameter. The following natural and synthetic standards were used for microprobe (WDS mode): fluorophlogopite (Si, Al, Mg, F), diopside (Ca), orthoclase (K, Al), albite (Na), chlorapatite (Cl), hematite (Fe), rutile (Ti), MnFe₂O₄ (Mn), anhydrite (S). Precisions for the major and minor elements were better than 2 and 5 rel. %, respectively. Data reduction was performed using a PAP routine. Overlap corrections were done for the following elements: SiKα – SrLα and BaLα – TiKα.

The trace-element composition (Be, Li, B, Rb, Ba, Th, Sr, Y, REE) of umbrianite was studied by secondary-ion mass spectroscopy (SIMS) on a Cameca IMS-4f ion probe at the Yaroslavl Branch of the Institute of Physics and Technology (YBIPT), Yaroslavl, Russia. For the analysis, umbrianite grains larger than 20 μm and previously analyzed by electron microprobe were selected. Analysis of trace elements was carried out by the energy filter method; operating conditions: primary O²⁻ beam – 20 μm, *I* = 2–4 nA, energy offset – 100 eV, and energy slit – 50 eV. Concentrations of elements were determined from the ratios of their isotopes to ³⁰Si, using calibration curves for standard samples (Jochum *et al.*, 2000). The hydrogen content was determined from the ¹H mass together with trace elements. A low background content of H₂O (0.03

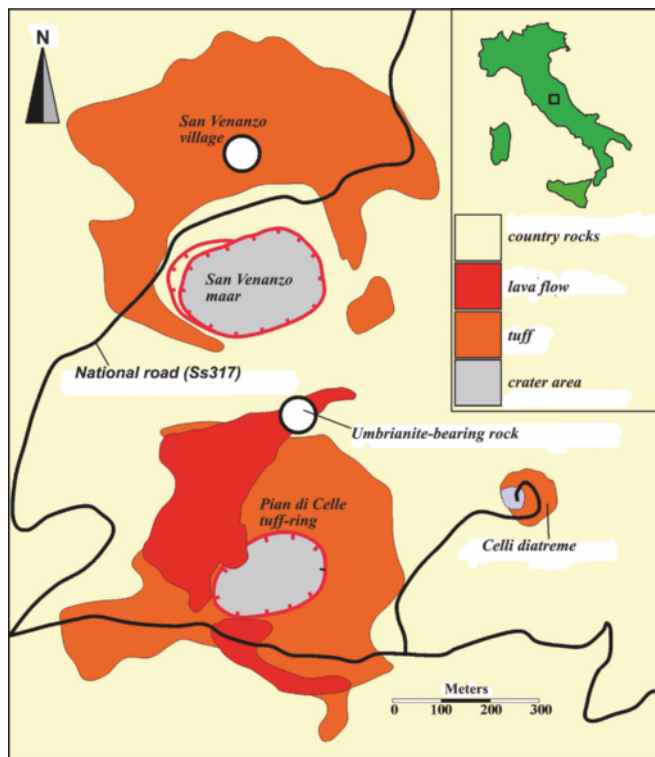


Fig. 1. Sketch map of the San Venanzo and Pian di Celle volcanoes.

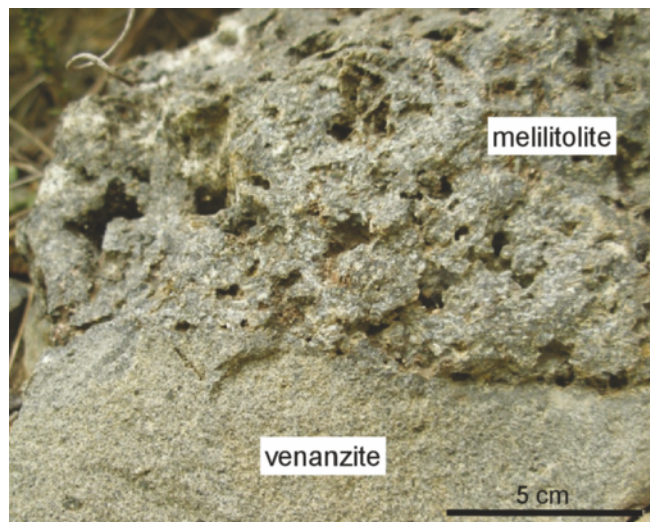


Fig. 2. Pegmatoid vesicular melilitolite in venanzite lava flow.

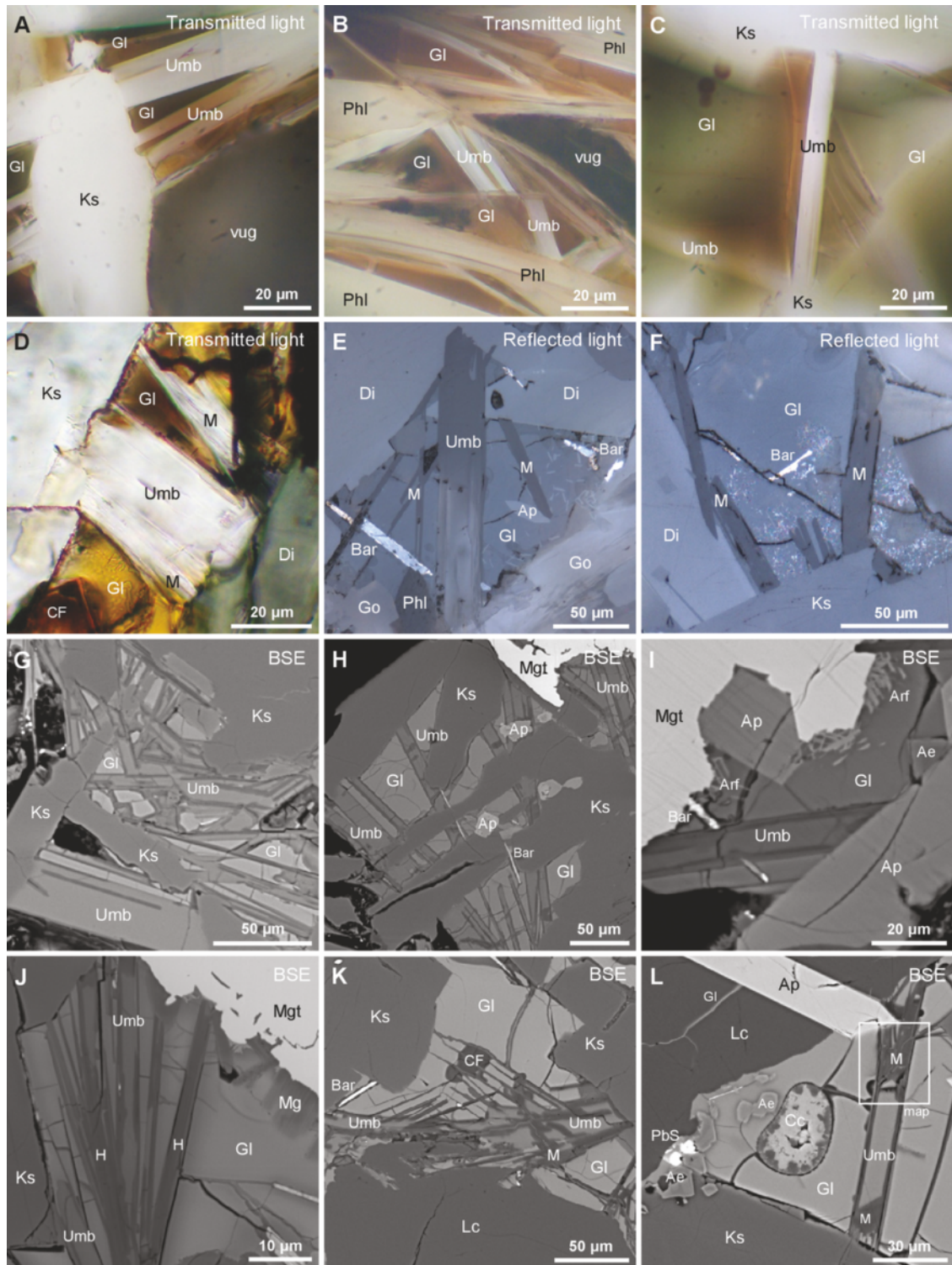


Fig. 3. Umbrianite in melilitolite (images in thin sections): Umb – umbrianite; Ks – kalsilite; Lc – leucite; Gl – silicate glass; Phl – fluorophlogopite; Mgt – Ti-rich magnetite; Ap – fluorapatite; Go – götzenite; Di – diopside; Ae – aegirine; Arf – arfvedsonite; H, M – Ba-rich hydrated phases; Bar – partially altered bartonite; Mg – Mg-H₂O-rich silicate; CF – hydrated Ca-Fe-silicate; Cc – calcite-fluorite globule; map – see Fig 8.

wt%) in the mass spectrometer was obtained through a 24 h high-vacuum exposure of the samples. The NIST610 glass was used as standard.

Single-crystal X-ray diffraction studies and crystal structure determination were performed using an Xcalibur S diffractometer equipped with a CCD detector

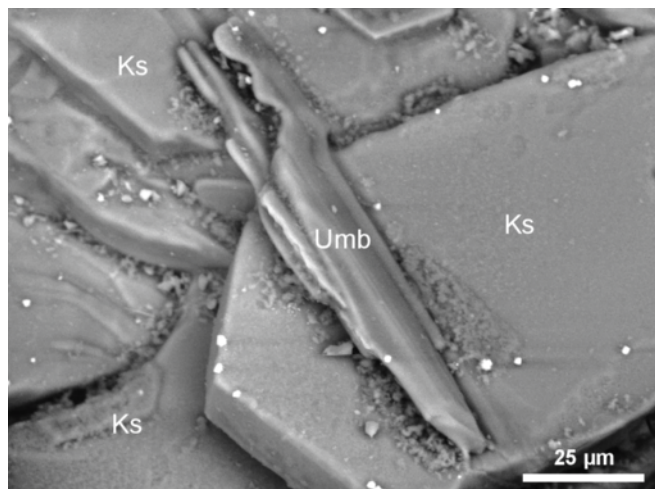


Fig. 4. Back-scattered electron image of a coarse crystal of umbrianite (Umb) on kalsilite (Ks) in a vug of melilitolite.

($\text{MoK}\alpha$ -radiation, $\lambda = 0.71073 \text{ \AA}$) at Moscow State University. X-ray powder diffraction data were obtained on a Stoe IPDS II diffractometer equipped with an image plate detector (St. Petersburg State University), using the Gandolfi method ($\text{MoK}\alpha$ radiation, 45 kV, 30 mA, 200 mm detector-to-sample distance, exposure 60 min). Data were processed with Stoe X-Area 1.42 and Stoe WinXPOW 2.08 program packages.

A LabRAM HR 800 mm spectrometer (Horiba Scientific) equipped with a Peltier-cooled CCD detector and an Olympus BX40 confocal microscope and a $100\times$ objective were used at IGM. The 514.5 nm line of a solid-state laser source and power of 50 mW were used for sample excitation. Raman spectra of umbrianite and related minerals were recorded in a backscattering geometry in the range $200\text{--}4000 \text{ cm}^{-1}$. Collection times of 10 s, accumulations of 15 scans and a $20 \mu\text{m}$ confocal hole were chosen. The monochromator was calibrated using the Raman scattering line of a silicon plate (520.7 cm^{-1}). The baseline correction was performed because of the mineral luminescence.

4. Sample description

Vesicular melilitolites (Fig. 2) contain tabular melilite (up to 5 cm), olivine ($\text{Fo}_{>60}$), leucite, fluorophlogopite and Ti-rich magnetite as essential minerals that resemble the fine-grained groundmass of the hosting venanzites. Interstices between essential minerals are filled with an aggregate of Ti-rich magnetite, fluorophlogopite, fluorapatite, nepheline, kalsilite, diopside, Zr- and Ti-disilicates (the cuspidine–hiortdahlite series members and götzenite), solid solutions of ferroan monticellite and magnesian kirschsteinite, umbrianite, fluorite–calcite globules and green to brown glass (Sharygin *et al.*, 1996a and b; Stoppa *et al.*, 1997;

Sharygin, 1999, 2001, 2012; Bellezza *et al.*, 2004). In addition, micrometer-sized rare and exotic minerals (usually $< 20 \mu\text{m}$) occur directly in the glass or as daughter phases of silicate-melt inclusions hosted by early minerals. They are westerveldite, sulphides (pyrrhotite, bartonite-chlorobartonite, galena), Na- and REE-rich perovskite and fluorapatite, khibinskite, ilmenite, Na-rich pyroxene and amphibole (Zr-bearing aegirine, arfvedsonite), K- and Ca-containing bario-oligite and a mineral of the bafertisite group. The Cr-rich mineral of the magnesioferrite–magnetite series occurs as inclusions in olivine. Green or brown silicate glass is an important constituent of the rock containing the holotype sample of umbrianite.

The majority of minerals occur as well-shaped crystals in numerous vugs (up to 3 cm in size). Some cavities also contain calcite, vanadinite, rhodosite, willhendersonite, chabazite-Ca, phillipsite-Ca, thomsonite-Ca and apophyllite. Some parts of the melilitolite dykelet may contain abundant large ocelli of calcite (up to 20 vol. % of the rock).

The alteration processes are not very significant and correspond to partial to complete replacement of bartonite by a Cu-Fe-hydrated sulphide, the appearance of a Ba-rich hydrated rim around umbrianite, colour changing of the groundmass glass from green to brown with the appearance of Ca-Fe- H_2O - and Mg- H_2O -silicates in brown glass (Stoppa *et al.*, 1997).

Umbrianite is one of the late-magmatic minerals and is usually localized in glass in association with leucite, kalsilite and fluorophlogopite (Fig. 3 and 4). Sometimes it occurs as a daughter phase in silicate-melt inclusions in leucite, kalsilite and melilite (Stoppa *et al.*, 1997; Sharygin, 1999, 2001). Umbrianite is unstable during postmagmatic alterations. The fresh mineral is common in green glass, whereas crystals in brown glass are partly or completely replaced by Ba-rich hydrated phases (Fig. 3D, F, J–L).

5. Morphology, optical and physical properties of umbrianite

The holotype umbrianite forms rectangular, lamellar or lath-shaped crystals (up to $25 \times 30 \times 200 \mu\text{m}$ in size), typically coarse and flattened on $\{010\}$, and their sheaf-like clusters (up to $200\text{--}500 \mu\text{m}$ across) in a groundmass of melilitolite (Fig. 3). Crystals and aggregates sometimes occur in the vugs of melilitolite (Fig. 4). Prismatic crystals have the forms $\{010\}$ (major), $\{001\}$ and $\{100\}$. No twinning was observed.

Umbrianite is colourless and transparent in thin sections, streak is white. The mineral is non-fluorescent in the UV and cathode rays. It has vitreous luster. The Mohs' hardness is ~ 5 , the micro-indentation hardness is $\text{VHN}_{20} = 405\text{--}568 \text{ kg/mm}^2$, mean 473 kg/mm^2 . Cleavage is perfect on (010) and distinct on (100) and (001) . Fracture is stepped to uneven across cleavage. Density was not measured directly because of the small

Table 1. Chemical composition of umbrianite in comparison with günterblässite and delhayelite.

	1	s.d.	Range	2	3	4	5	6	7	8	9	10	11	12
<i>n</i>	58			15	1	11	5	2	3	1	4	3	7	18
SiO ₂ wt%	42.83	0.35	42.15–43.58	42.74	42.65	42.22	42.26	42.95	43.17	43.20	42.94	42.85	52.94	47.12
TiO ₂	0.05	0.04	0.00–0.17	0.04	0.04	0.03	0.05	0.00	0.05	0.15	0.12	0.05		0.04
B ₂ O ₃ SIMS				0.08	0.06									0.04
Al ₂ O ₃	11.58	0.52	10.47–12.53	11.98	11.24	11.95	12.34	11.52	10.92	10.87	11.98	10.87	13.94	6.14
Fe ₂ O ₃	2.04	0.49	1.32–3.21	1.40	2.66	2.19	1.45	1.34	2.50	3.21	1.65	2.96	3.40	0.17
MnO	0.06	0.03	0.00–0.10	0.06	0.10	0.07	0.09	0.06	0.06	0.03	0.04	0.02		0.13
MgO	0.40	0.08	0.11–0.55	0.41	0.45	0.31	0.32	0.35	0.48	0.40	0.34	0.16	0.58	0.04
CaO	10.96	0.32	10.22–11.49	10.43	11.20	10.96	11.01	10.58	10.94	11.12	10.74	10.89	3.58	13.44
BaO	0.04	0.06	0.00–0.30	0.04	0.05	0.05	0.04	0.00	0.02	0.26	0.04	0.06	4.07	0.01
SrO	0.05	0.04	0.00–0.16	0.07	0.09	0.00	0.00	0.02	0.09	0.11	0.04	0.00		0.28
Na ₂ O	3.61	0.26	3.02–4.23	3.54	3.35	3.52	3.97	3.72	3.67	3.59	3.74	3.67	0.40	6.84
K ₂ O	22.55	0.28	21.67–23.03	22.57	22.59	22.76	21.67	23.03	22.89	22.57	22.62	22.65	5.18	19.91
Rb ₂ O SIMS				0.03										0.27
Li ₂ O SIMS				0.008	0.002									0.000
F	2.89	0.20	2.38–3.19	3.04	2.96	2.97	2.98	3.12	2.67	2.71	2.71	2.52		4.38
Cl	5.04	0.20	4.51–5.41	4.93	5.11	5.17	4.97	5.27	5.25	5.03	5.32	5.29		3.78
S	0.01	0.01	0.00–0.03	0.01		0.01	0.00	0.01	0.01	0.01	0.01	0.00		0.16
H ₂ O _{meas}				0.98	0.91								15.20	0.86
Total	102.37			102.36	103.46	102.49	101.51	102.02	102.77	103.53	102.60	102.28	84.09	103.60
O = (F,Cl) ₂	2.36			2.40	2.40	2.42	2.38	2.51	2.31	2.28	2.34	2.26		2.70
Total	99.76			99.96	101.06	99.80	98.75	99.46	100.43	100.99	99.95	99.72	84.09	100.90
Formula based on (Si,Al,Fe ³⁺) ₁₃ O ₂₉														
Si	9.598			9.572	9.559	9.471	9.490	9.704	9.689	9.612	9.574	9.624	9.568	6.910
Al	3.058			3.161	2.969	3.159	3.265	3.068	2.889	2.850	3.149	2.876	2.969	1.061
Fe ³⁺	0.342			0.236	0.449	0.370	0.245	0.228	0.422	0.538	0.277	0.500	0.462	0.019
B				0.031	0.023									0.010
Sum T	13.000			13.000	13.000	13.000	13.000	13.000	13.000	13.000	13.000	13.000	13.000	8.000
Ti	0.008			0.007	0.007	0.005	0.008	0.000	0.008	0.025	0.020	0.008		0.005
Mn	0.011			0.012	0.019	0.013	0.016	0.012	0.012	0.005	0.007	0.004		0.016
Mg	0.133			0.136	0.150	0.104	0.106	0.119	0.160	0.134	0.114	0.053	0.156	0.009
Ca	2.632			2.503	2.690	2.635	2.648	2.560	2.631	2.651	2.565	2.621	0.693	2.112
Sr	0.006			0.009	0.012	0.000	0.000	0.003	0.012	0.014	0.006	0.000		0.024
Ba	0.004			0.004	0.004	0.004	0.004	0.000	0.001	0.023	0.004	0.005	0.288	0.000
Na	1.568			1.537	1.456	1.531	1.727	1.630	1.598	1.549	1.617	1.597	0.140	1.946
K	6.447			6.449	6.459	6.515	6.209	6.639	6.554	6.406	6.436	6.489	1.194	3.725
Rb				0.004										0.025
Li				0.007	0.002									0.000
Sum K	10.810			10.668	10.798	10.809	10.719	10.962	10.978	10.807	10.768	10.777	2.472	7.861
F	2.050			2.153	2.098	2.107	2.118	2.226	1.893	1.907	1.913	1.792		2.031
Cl	1.914			1.873	1.941	1.967	1.892	2.018	1.998	1.897	2.010	2.012		0.939
S	0.004			0.004		0.003	0.001	0.006	0.004	0.005	0.004	0.002		0.044
	3.968			4.030	4.039	4.077	4.011	4.250	3.894	3.809	3.926	3.806		3.014
H ⁺				1.464	1.360								18.325	0.837

Notes: *n* – number of analyses; Li₂O, Rb₂O, B₂O₃ and H₂O in umbrianite and delhayelite are determined by SIMS. 1 – average composition of holotype umbrianite; 2–10 – individual grains of umbrianite (central part); 11 – günterblässite, Rother Kopf, Eifel, Germany, initial FeO was recalculated into Fe₂O₃ (Chukanov *et al.*, 2012a); 12 – delhayelite, Yukspor, Khibiny, Kola, Russia, formula is calculated on the basis of (Si + Al + Fe³⁺) = 8.

size of homogeneous grains. The calculated density is 2.49 g/cm³.

The mineral is optically biaxial (–); $\alpha = 1.537(2)$, $\beta = 1.543(2)$, $\gamma = 1.544(2)$ (589 nm), 2V (meas.) = 30(10), 2V (calc.) = 44.3. The optical orientation is: $X = b$; axes of the optical indicatrix are perpendicular to the cleavage planes. No dispersion and pleochroism were observed. Gladstone-Dale's compatibility factor for the holotype umbrianite is –0.051 (good).

6. Chemical composition

The chemical composition of the new mineral is given in Table 1. The empirical formula (based on Si + Al + Fe = 13 *apfu*) of the holotype umbrianite is (K_{6.45}Na_{0.35}(Sr,Ba)_{0.01})_{Σ6.81}(Na_{1.22}Ca_{0.78})_{Σ2.00}(Ca_{1.85}Mg_{0.13}Mn_{0.01}Ti_{0.01})_{Σ2.00}[(Fe³⁺)_{0.34}Al_{3.06}Si_{9.60}]_{Σ13.00}O_{29.00}F_{2.05}Cl_{1.91}(OH)_{0.04} (analysis 1, Table 1). The grouping of cations is according to the structure data. All iron is considered as Fe³⁺ on the basis

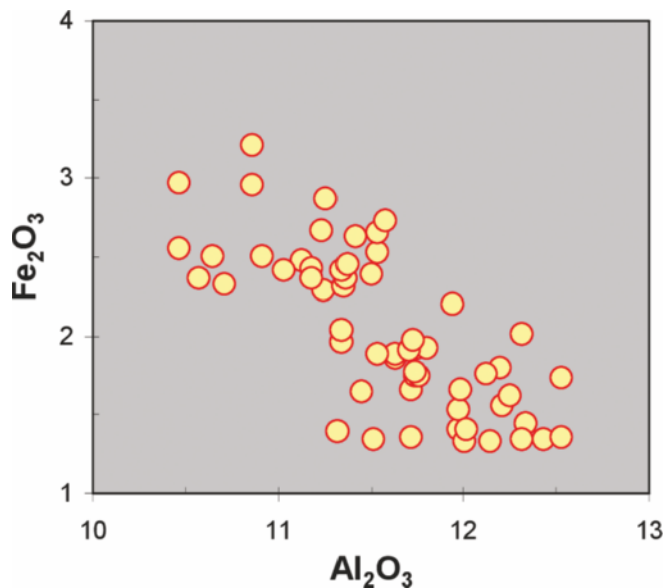


Fig. 5. Negative correlation between Al_2O_3 and Fe_2O_3 (in wt.%) in umbrianite.

of the structural data and of the distinct inverse correlation between Al and Fe observed for point analyses (Fig. 5). Umbrianite contains the following components in minor amounts (in wt%): TiO_2 – up to 0.2; MnO – up to 0.1; MgO – up to 0.55; BaO – up to 0.3; SrO – up to 0.15; S – up to 0.03.

The contents of H_2O and CO_2 were not determined directly because of the scarcity of available material. The absence of CO_2 and of any significant amount of H_2O is supported by the Raman spectroscopy (Fig. 6, the bands in the region of $1000\text{--}1150\text{ cm}^{-1}$ correspond to stretching vibrations of Si-O-Si) and structure data. The SIMS data for two crystals showed up to 1.0 wt% H_2O . However, the analyzed crystals (30–40 μm in size) contained hydrated rims that may have contaminated the analysis (beam diameter *ca.* 25 μm). Thus,

the actual H_2O content in fresh umbrianite is essentially lower than 1 wt%. In addition, SIMS data indicated the minor presence of some elements (in ppm): Sr – 1245–1610; Ba – 900–1960; B – 130–175; La – 8–15; Ce – 20–45; Nd – 10–29, Y – 30–70; Li – 7–20, Be – 55. The ideal formula of umbrianite is $\text{K}_7\text{Na}_2\text{Ca}_2[\text{Al}_3\text{Si}_{10}\text{O}_{29}]\text{F}_2\text{Cl}_2$, which requires K_2O 24.70, Na_2O 4.64, CaO 8.40, Al_2O_3 11.46, SiO_2 45.02, F 2.85, Cl 5.31, $\text{O} = (\text{F}, \text{Cl})_2 \cdot 2.40$, total 100.00 wt%. Figure 7 shows the chemical difference between umbrianite and Al-containing minerals of the rhodesite series.

The composition of hydrated rims around umbrianite crystals is strongly variable (Table 2) which suggests the presence of two different minerals. A Ba-rich phase, occasionally occurring around umbrianite, shows $b \approx 37.5\text{ \AA}$ (R. Wirth, personal communication), which is intermediate in this cell parameter between umbrianite and günterblassite. The Raman spectra support the assumption of a structural similarity of umbrianite and Ba-rich hydrated phase (Fig. 6). The simplified formula for such compositions (analyses 4–6, Table 2, Fig. 8) may be given as $(\text{K}, \text{Ba}, \text{Ca}, \text{Na})_{2-3}\text{Ca}_2[\text{Al}_3\text{Si}_{10}\text{O}_{25}(\text{OH}, \text{O})_4]\text{F}(\text{Cl}, \text{OH}) \cdot 6\text{--}7\text{H}_2\text{O}$ and is similar to günterblassite, $(\text{K}, \text{Ca}, \text{Ba}, \text{Na}, \square)_3\text{Fe}[(\text{Si}, \text{Al})_{13}\text{O}_{25}(\text{OH}, \text{O})_4] \cdot 7\text{H}_2\text{O}$ (Chukanov *et al.*, 2012a; Rastsvetaeva *et al.*, 2012). However, another cluster of analyses richer in CaO and poorer in Al_2O_3 (analyses 1–3, Table 2) is more correctly calculated as a delhayelite-typeminerals – $(\text{K}, \text{Ba}, \text{Ca}, \text{Na})_{1-2}\text{Ca}_2[\text{AlSi}_7\text{O}_{17}(\text{OH}, \text{O})_2](\text{F}, \text{Cl}, \text{OH})_{0-2} \cdot 4\text{--}5\text{H}_2\text{O}$ that is close to macdonaldite, $\text{BaCa}_4[\text{Si}_{16}\text{O}_{36}(\text{OH})_2] \cdot 10\text{H}_2\text{O}$ (Alfors *et al.*, 1965), and hydrodelhayelite, $\text{KCa}_2[\text{AlSi}_7\text{O}_{17}(\text{OH})_2] \cdot 6 - x\text{H}_2\text{O}$ (Dorfman & Chiragov, 1979; Ragimov *et al.*, 1980).

7. X-ray crystallography and crystal structure of umbrianite

The X-ray diffraction powder data for umbrianite are given in Table 3. The unit-cell parameters calculated from the powder-diffraction data are: $a = 7.071(6)$, $b = 38.50(6)$, $c = 6.574(7)$

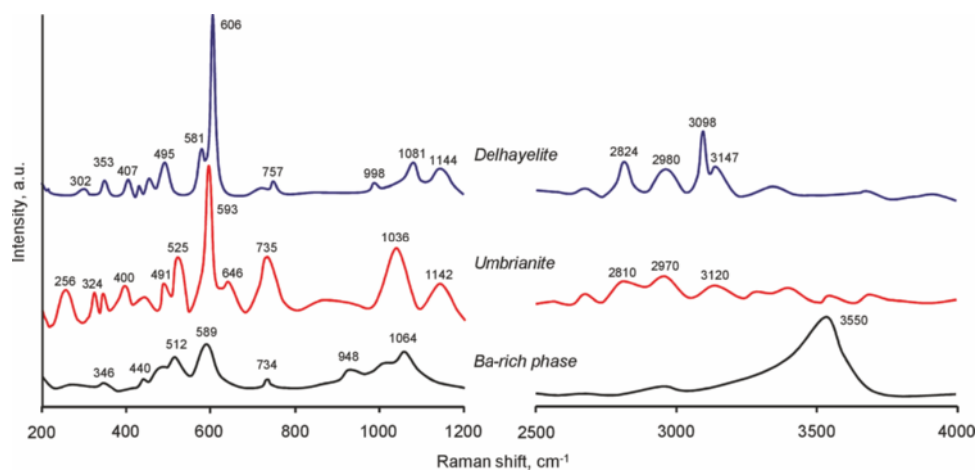


Fig. 6. Raman spectra of umbrianite (an. 9, Table 1), a Ba-rich phase (alteration product of umbrianite, an. 6, Table 2) and delhayelite (an. 12, Table 1). The bands in the region of $1000\text{--}1150\text{ cm}^{-1}$ correspond to stretching vibrations of Si-O-Si.

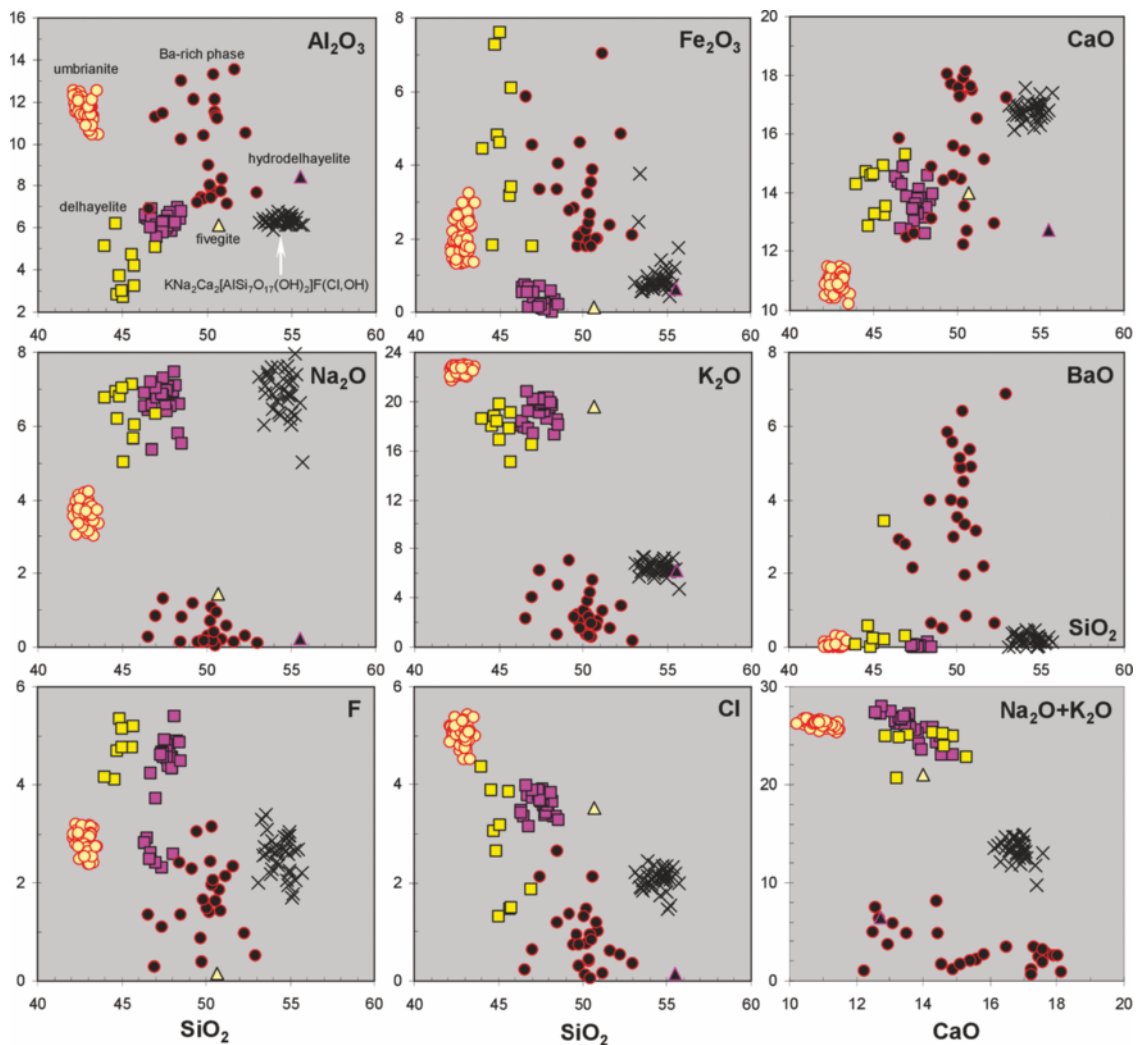


Fig. 7. Compositional variations (in wt.%) of umbrianite and related Ba-rich phases (alteration products of umbrianite) in comparison with the Al-containing members of the rhodesite series.

Circles - umbrianite (yellow/light) and hydrated Ba-rich phases (dark) from melilitolites, Pian di Celle, Italy; squares - delhayelite from peralkaline rocks, Khibiny, Kola, Russia (lilac/dark) and from peralkaline nephelinite, Oldoinyo Lengai, Tanzania (yellow/light); light/yellow triangle - figevite from peralkaline pegmatites, Khibiny; dark triangle - hydrodelhayelite from hydrothermally altered peralkaline pegmatites, Khibiny; crosses - a delhayelite-group mineral with formula close to $(\text{KNa}_2\text{Ca}_2[\text{AlSi}_7\text{O}_{17}(\text{OH})_2]\text{F}(\text{Cl},\text{OH}))$ from nephelinite, Sadiman, Tanzania, and from peralkaline phonolite, Sangro, SE Morocco. The HRTEM data for the Sadiman sample have shown that b parameter is $\approx 24.1 \text{ \AA}$ (R. Wirth, personal communication). New author's data and data from Dorfman (1958), Dorfman & Chiragov (1979), Stoppa *et al.* (1997), Dawson (1998), Dawson & Hill (1998), Ageeva (2002), Sharygin (2002), Sokolova *et al.* (2005), Berger *et al.* (2009), Pekov *et al.* (2009, 2011), Sharygin *et al.* (2012) and Zaitsev *et al.* (2012) were used for the plots.

\AA , $V = 1790(6) \text{ \AA}^3$. The single-crystal X-ray study shows orthorhombic symmetry, space group $Pmnm$, $a = 7.0618(5)$, $b = 38.420(2)$, $c = 6.5734(4) \text{ \AA}$, $V = 1783.5(2) \text{ \AA}^3$, $Z = 2$. The structure was solved by direct methods and refined on the basis of 1372 independent reflections with $I > 2\sigma(I)$ to $R = 0.0941$ with the use of SHELX software package (Sheldrick, 2008). The crystal data and the structure refinement details are given in Table 4, atom coordinates and equivalent displacement parameters in Table 5 and selected interatomic distances in Table 6. Relatively high value of R and disorder of oxygen position O(8) caused our attempt to refine the umbrianite structure in the acentric space group $Pm2_1n$ found for the closely related günterblässite (Rastsvetaeva *et al.*, 2012). However, the refinement did not lead to better R value and

the splitting of O position remained in the resulting model. Thus, the space group $Pmnm$ was chosen.

Umbrianite is a representative of a new structure type. Its crystal structure (Table 5, Fig. 9) contains a block consisting of triple tetrahedral layers formed by four- and eight-membered rings of tetrahedra (T) centred by Si and Al (with minor Fe). Two outer layers $[T_4O_{10}]$ formed by the Si(3), Si(4) and Al tetrahedra are topologically identical to that in double-layer silicates of the rhodesite mero-pleisotype series, namely rhodesite, delhayelite, figevite, hydrodelhayelite, macdonaldite and monteregianite-(Y) (Cadoni & Ferraris, 2009; Pekov *et al.*, 2009, 2011) (Figs. 10 and 11b) and in the single-layer phyllosilicates cryptophyllite (Fig. 11a) and shlykovite, belonging to the mountainite family (Pekov *et al.*, 2010;

Table 2. Chemical composition of Ba-rich phases replacing umbrianite.

<i>n</i>	1	2	3	4	5	6
	<i>l</i>	<i>3</i>	<i>4</i>	<i>l</i>	<i>l</i>	<i>3</i>
SiO ₂ wt%	52.99	50.23	50.26	49.84	45.79	47.95
TiO ₂	0.07	0.06	0.03	0.35	0.13	0.16
Al ₂ O ₃	7.67	7.51	8.17	10.37	11.58	10.53
Fe ₂ O ₃	2.10	2.25	2.01	4.59	2.38	3.77
MnO	0.13	0.23	0.08	0.04	0.04	0.03
MgO	0.40	0.42	0.31	0.74	0.36	0.39
CaO	17.24	17.85	16.98	14.57	14.20	13.38
BaO	6.86	5.87	4.71	2.99	2.22	4.68
SrO	0.75	0.00	0.00	0.37	0.26	0.00
Na ₂ O	0.10	0.18	0.34	0.18	0.78	1.52
K ₂ O	0.52	2.18	2.44	1.50	5.86	4.65
F	0.51	2.68	1.17	1.65	1.90	0.96
Cl	0.35	0.78	1.02	0.73	2.27	0.94
S		0.03	0.01	0.04	0.02	0.00
Total	89.69	90.26	87.52	87.96	87.78	88.96
O = (F,Cl) ₂	0.29	1.30	0.72	0.86	1.31	0.62
Total	89.40	88.96	86.80	87.10	86.47	88.34

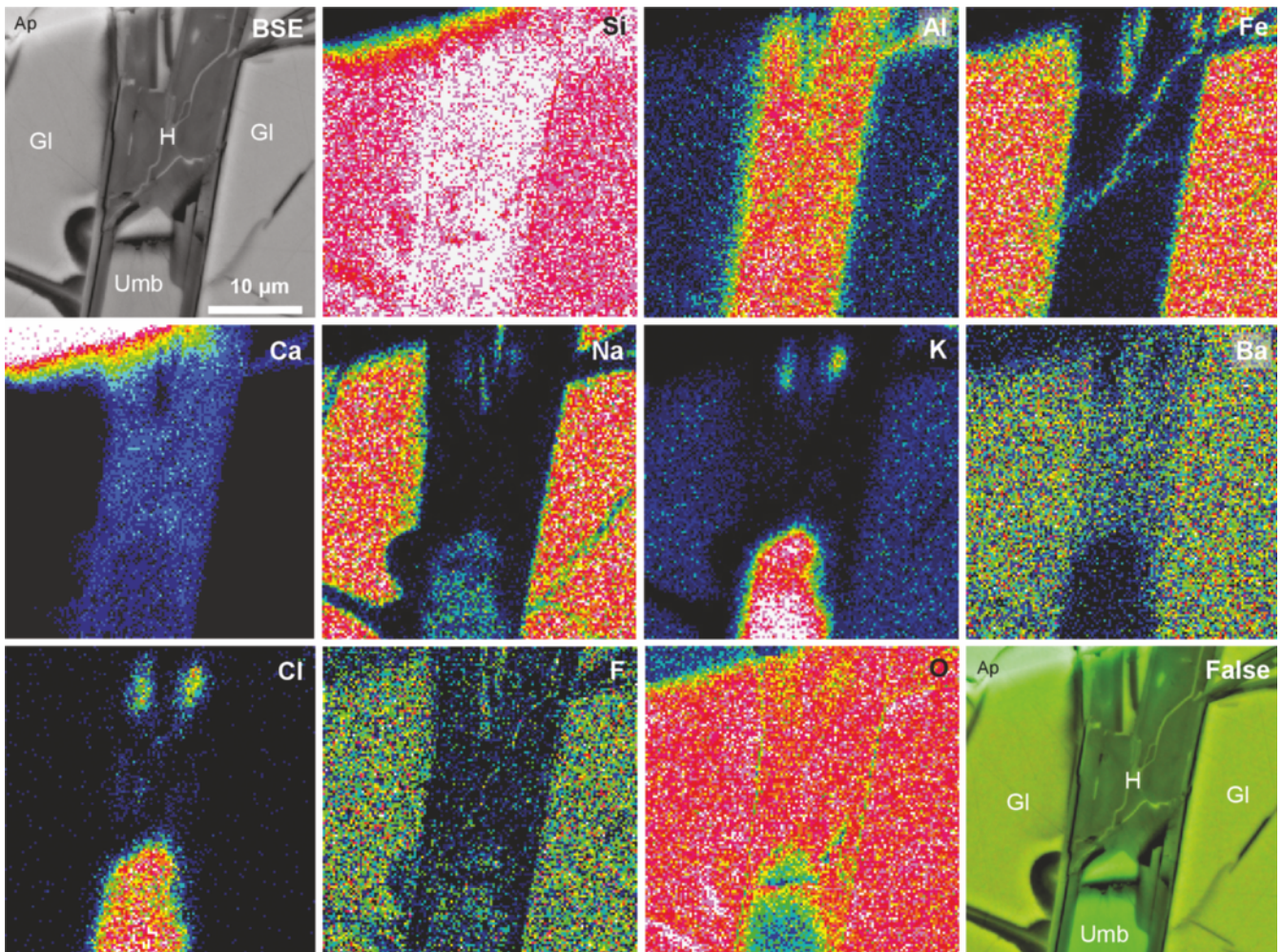


Fig. 8. Elemental maps for umbrianite partially replaced by a Ba-rich hydrated phase. See Fig. 3 L for details.

Table 3. X-ray powder-diffraction data of umbrianite.

I_{obs}	d_{obs} , Å	I_{calc}^*	d_{calc}^{**} , Å	hkl
100	9.65	38	9.605	040
43	6.91	40	6.945	110
97	6.59	9	6.573	001
24	5.06	16	4.995	051
18	4.63	7	4.587	061
25	3.884	6	3.878	081
77	3.296	33, 16, 4, 41	3.317, 3.314, 3.287, 3.275	0.10.1, 240, 002, 012
70	3.118	28, 91, 37	3.131, 3.100, 3.092	1.11.0, 211, 260
52	2.903	80, 12, 100, 30	2.924, 2.902, 2.883, 2.878	062, 132, 251, 0.12.1
53	2.819	74, 34	2.826, 2.798	1.11.1, 261
15	2.731	2, 15	2.744, 2.726	0.14.0, 1.13.0
12	2.621	2, 18	2.619, 2.611	172, 281
13	2.414	22	2.418	2.10.1
10	2.179	9	2.181	1.12.2
23	2.089	5, 9	2.098, 2.058	1.13.2, 2.14.1
8	2.003	4, 1, 5, 12	2.039, 2.030, 1.986, 1.981	2.10.2, 0.18.1, 2.16.0, 2.11.2
8	1.906	4, 6, 14	1.904, 1.903, 1.901	322, 0.10.3, 2.16.1
21	1.859	27, 4, 9	1.862, 1.856, 1.853	203, 0.11.3, 223
16	1.781	16, 5, 36	1.790, 1.771, 1.765	0.18.2, 1.21.0, 400
15	1.698	10	1.699	2.16.2
9	1.574	3, 1, 1, 7, 7	1.582, 1.579, 1.578, 1.573, 1.567	3.17.1, 144, 1.16.3, 0.17.3, 154
9	1.543	8	1.546	4.12.0
4	1.442	1, 4	1.444, 1.442	3.21.0, 4.10.2
4	1.368	9, 2	1.370, 1.365	2.11.4, 1.27.1
4	1.204	1, 1, 3, 1	1.206, 1.205, 1.203, 1.202	3.21.3, 1.21.4, 404, 275
3	1.124	1, 3, 1, 1	1.126, 1.125, 1.122, 1.121	681, 5.17.2, 1.17.5, 3.19.4
3	1.109	2	1.109	6.10.1
3	1.084	1, 1	1.085, 1.085, 1.083	3.21.4, 056, 5.22.1
3	1.064	1, 1, 2	1.067, 1.063, 1.062	2.18.5, 1.27.4, 2.34.1

*Only reflections with $I_{\text{calc}} \geq 1$ are given.

**Calculated for unit-cell parameters obtained from single-crystal data.

Table 4. Crystal data, data-collection information and refinement details for umbrianite.

Formula	$\text{K}_{13.8}(\text{Na}_{0.75}\text{Ca}_{0.25})_4\text{Ca}_4[\text{Al}_4(\text{Si}_{0.5}\text{Al}_{0.5})_2(\text{Si}_{0.55}\text{Al}_{0.30}\text{Fe}^{3+}_{0.15})_4\text{Si}_{16}\text{O}_{58}]\text{F}_4\text{Cl}_4$
Formula weight	2669.75
Space group, Z	$Pm\bar{m}n$, 1
Unit-cell dimensions	$a = 7.0618(5)$ Å $b = 38.420(2)$ Å $c = 6.5734(4)$ Å
Volume	$1783.46(19)$ Å ³
Density (calculated)	2.486 g/cm ³
μ	1.943 mm ⁻¹
$F(000)$	1316
Crystal size	$0.05 \times 0.09 \times 0.19$ mm
Data collection	Xcalibur S CCD
Temperature	293(2) K
Radiation, wavelength	$\text{MoK}\alpha$, $\lambda = 0.71073$ Å
θ range for data collection	2.93 – 28.28°
h, k, l ranges	$-9 \leq h \leq 9$, $-51 \leq k \leq 51$, $-8 \leq l \leq 8$
Reflections collected	43758
Unique reflections	2417
Reflections with $I > 2\sigma(I)$	1372
Structure solution	direct methods
Refinement method	full-matrix least-squares on F^2
Number of refined parameters	168
Weighting scheme	$1/[\sigma^2(F_o^2) + (0.0945P)^2 + 0.00P]$, $P = [\max(F_o^2) + 2(F_c)^2]/3$
$R_F [I > 2\sigma(I)]/wR(F^2) [I > 2\sigma(I)]$	0.0941/0.1881
GoF	1.123
$\Delta\rho_{\text{max}}/\Delta\rho_{\text{min}}$	$0.855/-0.830$ e/Å ³

Table 5. Atom coordinates and equivalent displacement parameters (U_{eq} , Å²), site multiplicities (Q) and site occupancy factors (s.o.f.) in the structure of umbrianite.

Atom	x	y	z	U_{eq}	Q	s.o.f.
K(1)	0.25	0.33849(9)	0.1112(8)	0.0617(13)	4	K _{1.00}
K(2)	0.25	0.25	-0.2775(9)	0.0351(14)	2	K _{0.80} Na _{0.08}
K(3)	0.25	0.41285(8)	-0.2824(6)	0.0353(10)	4	K _{0.90} Na _{0.06}
K(4)*	0.25	0.6602(2)	0.5198(14)	0.035(2)**	4	K _{0.45}
K(4')*	0.1570(18)	0.6603(3)	0.523(2)	0.049(3)**	8	K _{0.25}
Na	0.0	0.5	0.5	0.0232(10)	4	Na _{0.70} Ca _{0.30}
Si(1)	0.25	0.75	0.3961(8)	0.0144(12)	2	Si _{0.50} Al _{0.50}
Si(2)	0.25	0.70109(8)	0.0231(6)	0.0234(10)	4	Si _{1.00}
Si(3)	0.25	0.56856(9)	-0.5795(5)	0.0155(8)	4	Si _{1.00}
Si(4)	-0.0330(3)	0.57166(6)	-0.2193(4)	0.0114(5)	8	Si _{1.00}
Si(5)	-0.0157(5)	0.75	0.7805(6)	0.0283(9)	4	Si _{0.55} Al _{0.30} Fe _{0.15}
Al	0.25	0.61619(9)	0.0332(6)	0.0165(9)	4	Al _{1.00}
Ca	0.25	0.50431(6)	-0.9977(4)	0.0111(6)	4	Ca _{0.95} Mg _{0.05}
O(1)	0.0631(14)	0.7146(2)	0.9075(15)	0.078(4)	8	1
O(2)	0.0512(13)	0.6023(2)	-0.0887(14)	0.066(3)	8	1
O(3)	0.25	0.5317(2)	-0.6820(14)	0.028(3)	4	1
O(4)	0.25	0.6021(2)	-0.7239(16)	0.046(3)	4	1
O(5)	-0.0169(10)	0.53449(17)	-0.1226(14)	0.049(2)	8	1
O(6)	0.25	0.6595(2)	0.0332(17)	0.070(5)	4	1
O(7)	0.0582(15)	0.75	0.5386(16)	0.051(3)	4	1
O(8)	0.75	0.75	0.797(3)	0.116(10)***	2	1
O(9)	0.0633(11)	0.5726(2)	-0.4375(10)	0.053(2)	8	1
O(10)	0.25	0.7153(2)	0.2564(14)	0.044(3)	4	1
O(11)	0.75	0.5826(2)	-0.2625(17)	0.036(3)	4	1
F	0.25	0.47937(18)	-1.3176(12)	0.0247(19)	4	1
Cl	0.75	0.66536(13)	0.3855(11)	0.099(2)	4	Cl _{0.95} F _{0.05}

*Closely located (see Fig. 9) sites K(4) and K(4') cannot be occupied simultaneously.

** U_{iso} .

***O(8) may be split (moved from the m plane, in the same space group $Pmmn$) from position $2a$ to $4e$ with coordinates 0.75, 0.7394(4), 0.796(3) and occupancy 0.5; this will lead to $U_{eq} = 0.039(6)$ Å².

Table 6. Selected interatomic distances (Å) in the structure of umbrianite.

Site	Site	Site	Site
K(1) – O(1) 3.011(8) × 2	K(4) – O(10) 2.736	Si(1) – O(10) 1.618(9) × 2	Al – O(6) 1.666(10)
O(2) 3.118(8) × 2	O(4) 2.747(13)	O(7) 1.647(11) × 2	O(4) 1.686(11)
O(11) 3.190(11)	O(6) 3.199(15)	Mean 1.6325	O(2) 1.703(8) × 2
Cl 3.269(9)	O(6) 3.375(15)		Mean 1.6895
Cl 3.311(9)	O(1) 3.550(14) × 2	Si(2) – O(6) 1.598(10)	
O(8) 3.454(5)	O(9) 3.625(12) × 2	O(1) 1.609(9) × 2	Ca – F 2.311(8)
O(6) 3.657(3) × 2	Cl 3.645(3) × 2	O(10) 1.628(9)	O(3) 2.327(9)
Mean 3.280	Mean 3.370	Mean 1.611	O(5) 2.357(7) × 2
			O(5) 2.360(7) × 2
			Mean 2.345
K(2) – O(7) 2.772(11) × 2	K(4') – O(10) 2.822(16)	Si(3) – O(3) 1.569(9)	
O(8) 3.16(2)	O(4) 2.839(16)	O(4) 1.601(10)	
Cl 3.328(5) × 2	Cl 3.018(13)	O(9) 1.622(8) × 2	Na – F 2.276(5) × 2
O(8) 3.41(2)	O(6) 3.285(17)	Mean 1.6035	O(3) 2.456(6) × 2
O(1) 3.558(12) × 4	O(1) 3.345(17)		O(5) 2.815(9) × 2
Mean 3.300	O(6) 3.419(17)	Si(4) – O(5) 1.567(6)	O(9) 2.855(9) × 2
	O(9) 3.444(15)	O(2) 1.573(7)	Mean 2.6005
	O(2) 3.471(17)	O(9) 1.588(7)	
K(3) – F 2.566(8)	O(7) 3.517(12)	O(11) 1.614(4)	
O(9) 2.932(8) × 2	Mean 3.240	Mean 1.5855	
O(11) 2.996(11)			
Cl 3.080(6)			
O(2) 3.288(11) × 2		Si(5) – O(8) 1.658(4)	
O(4) 3.5777(15) × 2		O(7) 1.674(11)	
O(11) 3.586(12)		O(1) 1.690(8) × 2	
Mean 3.182		Mean 1.678	

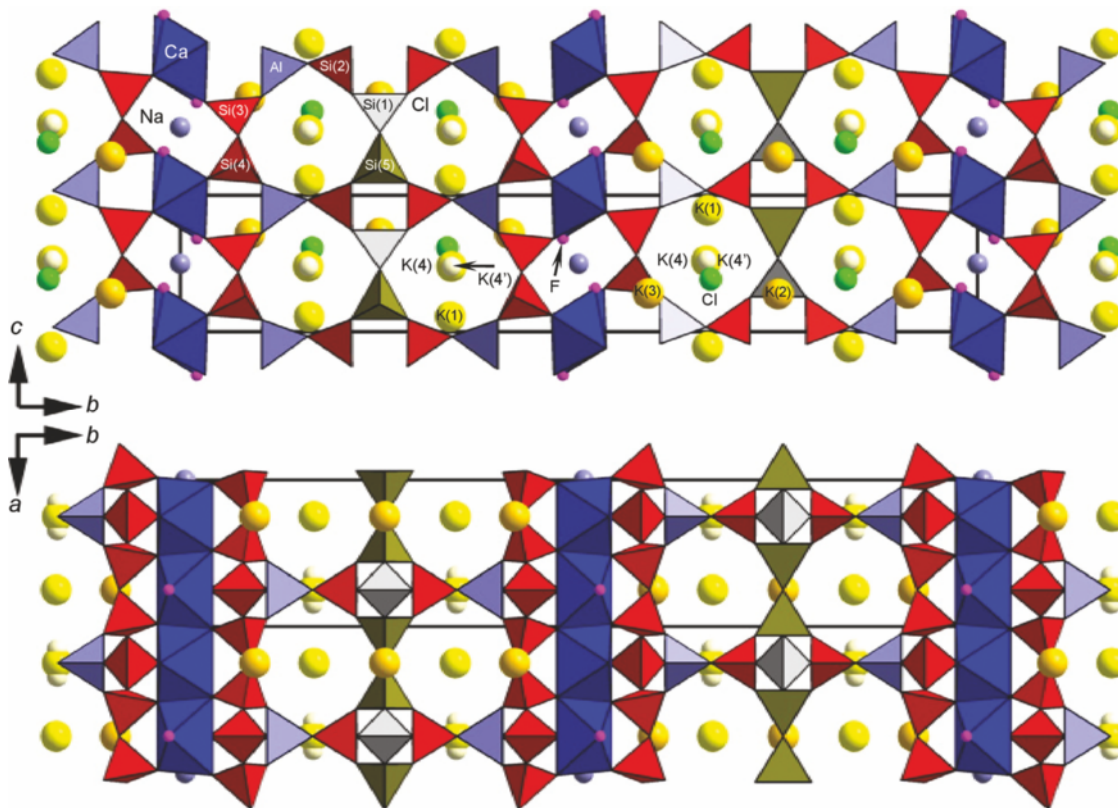


Fig. 9. Crystal structure of umbrianite in *bc* and *ab* projections. The unit cell is outlined.

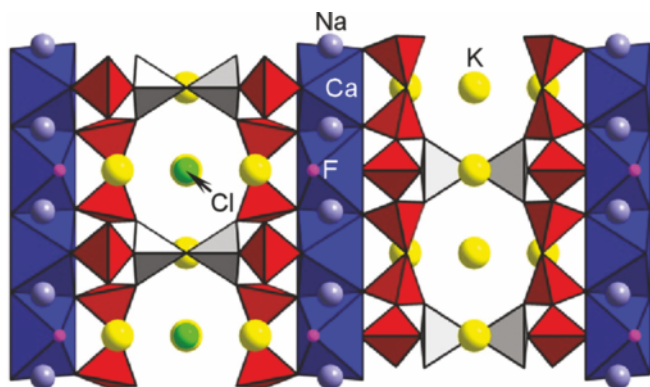


Fig. 10. Crystal structure of delhayelite, *ab* projection (Pekov *et al.*, 2009).

Zubkova *et al.*, 2010). The third (inner) layer [T_5O_{11}] in umbrianite consists of Si(1) = (Si,Al), Si(5) = (Si,Al,Fe) and Si(2) tetrahedra. Thus, the triple-layer tetrahedral block in umbrianite (Figs. 9 and 11c) has the formula $[Al_4(Si,Al)_2(Si,Al,Fe)_4Si_{16}O_{58}]^\infty$. It is topologically identical to that found in the recently discovered günterblässite, $(K,Ca,Ba,Na,\square)_3Fe[(Si,Al)_{13}O_{25}(OH,O)_4] \cdot 7H_2O$ (Chukanov *et al.*, 2012a; Rastsvetaeva *et al.*, 2012), and hillesheimite, $(K,Ca,Ba,\square)_2(Mg,Fe,Ca,\square)_2[(Si,Al)_{13}O_{23}(OH)_6](OH) \cdot 8H_2O$ (Chukanov *et al.*, 2012b). Unlike umbrianite, in günterblässite and hillesheimite all tetrahedra

are characterized by Si,Al disorder and the pending O vertices of the outer layers are protonated, thus represented by OH groups. Thus, the general formula of their triple-layer tetrahedral blocks is $[(Si,Al)_{26}O_{50}(OH,O)_8]^\infty$ in günterblässite and $[(Si,Al)_{26}O_{46}(OH)_{12}]^\infty$ in hillesheimite.

The tetrahedral blocks in umbrianite are linked to each other via columns of edge-sharing CaO_5F octahedra to form a 3D quasi-framework with channels filled by Cl^- and K^+ ions (both occur inside the tetrahedral blocks) and Na^+ ions (located between the Ca octahedral columns; Fig. 9). The arrangement of Ca^{2+} , Na^+ , K^+ , F^- and Cl^- ions in umbrianite (Fig. 9) is similar to that in the chemically and structurally related delhayelite (Fig. 10). The main difference between these minerals is in the structure of the tetrahedral blocks (double-layer in delhayelite and triple-layer in umbrianite) that causes their different chemical compositions (Si:Al, K:Na:Ca and F:Cl ratios), unit-cell dimensions (the *b* parameter), X-ray powder diffraction patterns and optical properties (Table 7). In summary, the structural formula of umbrianite is $(K_{6.5}Na_{0.2})_{\Sigma 6.7}(Na_{1.4}Ca_{0.6})_{\Sigma 2.0}(Ca_{1.90}Mg_{0.1})_{2.0\Sigma 2}[Fe^{3+}_{0.3}Al_{3.1}Si_{9.6}O_{29}]F_{2.05}Cl_{1.95}$ (Table 5), which is very close to the empirical formula (Table 1).

8. Genetic relations of umbrianite with other species

Umbrianite and some members of the rhodesite meroplesiotype series are genetically related, being formed in

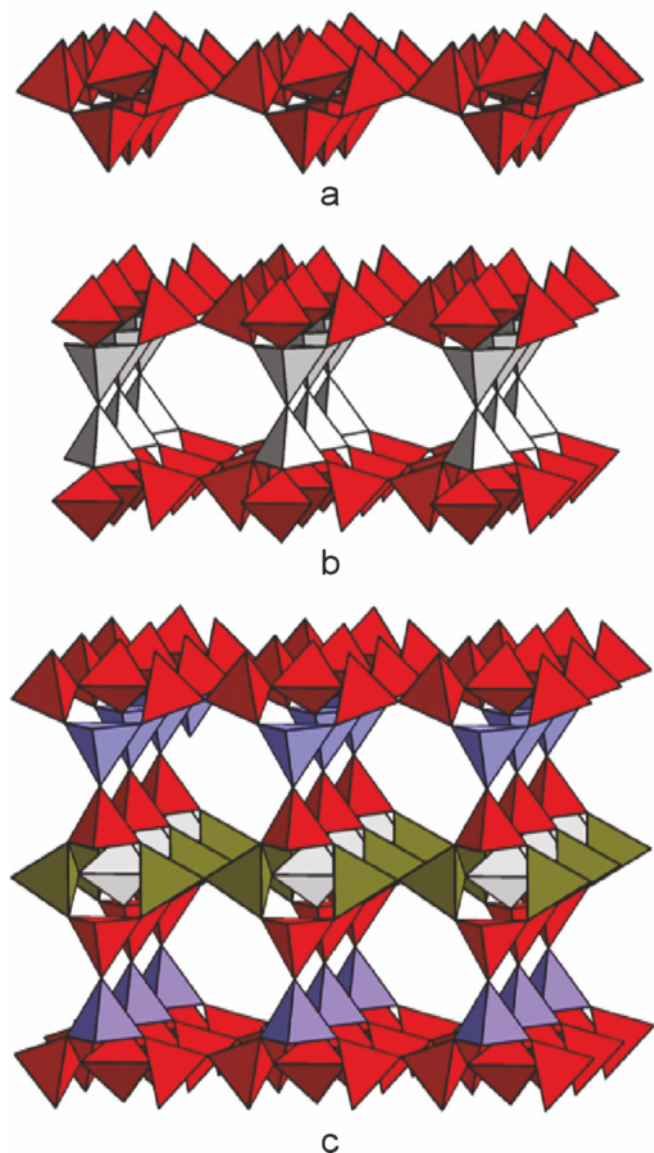


Fig. 11. Tetrahedral motifs in the crystal structures of related minerals: (a) single layer $[\text{Si}_4\text{O}_{10}]^\infty$ in cryptophyllite (Zubkova *et al.*, 2010), (b) double-layer block $[(\text{Si},\text{Al})_4\text{Si}_{12}\text{O}_{38}]^\infty$ in delhayelite (Pekov *et al.*, 2009) and (c) triple-layer block $[\text{Al}_4(\text{Si},\text{Al})_2(\text{Si},\text{Al},\text{Fe})_4\text{Si}_{16}\text{O}_{58}]^\infty$ in umbrianite. Colouring corresponds to that in Figs. 9 and 10.

young K-rich peralkaline volcanic rocks (Sahama & Hytönen, 1959; Stoppa *et al.*, 1997; Dawson & Hill, 1998; Sharygin, 1999, 2001; Berger *et al.*, 2009; Andersen *et al.*, 2012; Sharygin *et al.*, 2012; Zaitsev *et al.*, 2012). They commonly occur as late-magmatic minerals. Günterblässite and hillesheimite, which are structurally related with umbrianite (they contain the same type of tetrahedral anion), were found in hydrothermally altered young alkaline lavas of the Eifel volcanic region, Germany (Chukanov *et al.*, 2012a and b). Delhayelite, $\text{K}_4\text{Na}_2\text{Ca}_2[\text{AlSi}_7\text{O}_{19}]\text{F}_2\text{Cl}$, is very unstable in post-magmatic aqueous solutions, especially under weakly alkaline conditions, and alters to fivegite,

$\text{K}_4\text{Ca}_2[\text{AlSi}_7\text{O}_{17}(\text{O}_{2-x}\text{OH}_x)][(\text{H}_2\text{O})_{2-x}\text{OH}_x]\text{Cl}$, and further to hydrodelhayelite, $\text{KCa}_2[\text{AlSi}_7\text{O}_{17}(\text{OH})_2] \cdot 6 - x \text{H}_2\text{O}$, which is accompanied by leaching of alkali cations and halogen anions and hydration. In the course of these transformations, the CaAlSiO motif remains stable (Pekov *et al.*, 2011). The $\text{KNa}_2\text{Ca}_2[\text{AlSi}_7\text{O}_{17}(\text{OH})_2] \text{F}(\text{Cl},\text{OH})$ phase found in K-rich peralkaline rocks in Tanzania and Morocco (Berger *et al.*, 2009; Zaitsev *et al.*, 2012) seems to be intermediate between delhayelite and hydrodelhayelite.

Umbrianite shows similar behaviour under post-magmatic conditions. We assume that günterblässite is a product of alteration of a hypothetical umbrianite-like phase with Al,Si-disordered tetrahedral blocks. Thus, günterblässite can be considered as a genetic analogue of hydrodelhayelite, being in the same genetic relationship with a mineral close to umbrianite, as in the evolution series from delhayelite to hydrodelhayelite (see also Table 7). It is quite possible that one of the Ba-rich hydrated phases (Table 2, Fig. 3 and 8) identified by electron microprobe in replacement rims around umbrianite is an Al,Si-ordered structural analogue of günterblässite. Raman spectroscopy demonstrates the structural similarity between this phase and umbrianite (Fig. 6). However, another Ba-rich phase seems to be close in chemical composition to macdonaldite and hydrodelhayelite, double-layer silicates of the rhodesite series. Nevertheless, detailed structural studies are needed in order to demonstrate possible relations between umbrianite and Ba-rich phases from the alteration rims. In general, umbrianite, günterblässite and hillesheimite, three members of the günterblässite group, are remotely related, from the structural point of view, to minerals of the rhodesite mero-pleisotype series with double tetrahedral layers (Hesse *et al.*, 1992; Cadoni & Ferraris, 2009) and to minerals of the mountainite family with single tetrahedral layers (Zubkova *et al.*, 2010). Chemically, umbrianite is similar to delhayelite; the main differences are in the Al:Si ratio and the Na content (Tables 1 and 7). Both minerals are similar in a nearly complete occupancy of all possible positions.

9. Origin of umbrianite

Mineral phase relationships in the Pian di Celle melilitolite demonstrate that umbrianite is one of the late-magmatic phases. It is localized in the groundmass glass and is closely associated with westerveldite, sulphides, Na-rich pyroxene, amphibole and fluorite-carbonate globules (Fig. 3). The presence of umbrianite as a daughter phase in partially or completely crystallized silicate-melt inclusions in some major minerals (leucite, kalsilite and melilite) allows one to estimate its crystallization temperature.

Melt inclusions (5–70 μm) have been identified in both phenocrystal and groundmass minerals of the Pian di Celle melilitolite (Sharygin *et al.*, 1996a and b; Stoppa *et al.*, 1997; Sharygin, 1999, 2001). In phenocrysts (melilite, olivine, leucite), the silicate-melt inclusions are mainly localized in the outer zones, whereas, in the groundmass minerals (nepheline, kalsilite, apatite and others), they are situated in the central zones. Their phase composition is green glass + shrinkage fluid bubble \pm carbonate globule \pm trapped/daughter crystals.

Table 7. Comparative data for umbrianite and related minerals.

Mineral	Umbrianite	Günterblässite	Hillesheimite	Delhayelite
Formula	$K_7Na_2Ca_2 [Al_3Si_{10}O_{29}]F_2Cl_2$	$(K,Ca,Ba,Na,\square)_3Fe [(Si,Al)_{13}O_{25}(OH,O)_4](H_2O)_7$	$(K,Ca,\square)_2(Mg,Fe,Ca,\square)_2 [(Si,Al)_{13}O_{23}(OH)_6](OH)(H_2O)_8$	$K_4Na_2Ca_2 [AlSi_7O_{19}]F_2Cl$
Crystal system	Orthorhombic	Orthorhombic	Orthorhombic	Orthorhombic
Space group	$Pmmn$	$Pm2_1n$	$Pmmn$	$Pmmn$
Tetrahedral AlSiO block	Triple-layer with partial Al,Si-order: $[Al_4(Si,Al)_2(Si,Al,Fe)_4Si_{16}O_{58}]^\infty$	Triple-layer with Al,Si-disorder: $[(Si,Al)_{26}O_{50}(OH,O)_8]^\infty$	Triple-layer with Al,Si-disorder: $[(Si,Al)_{26}O_{46}(OH,O)_{12}]^\infty$	Double-layer with partial Al,Si-order: $[(Si,Al)_4Si_{12}O_{38}]^\infty$
$a, \text{Å}$	7.062	6.970	6.979	7.058
$b, \text{Å}$	38.420	37.216	37.182	24.579
$c, \text{Å}$	6.574	6.528	6.530	6.581
$V, \text{Å}^3$	1783.5	1693.3	1694	1141.6
Z	2	2	2	2
Major chemical constituents, wt%				
K_2O	21.7–23.0	5.2	4.2	18–21
Na_2O	3.0–4.2	0.4	0.2	6.6–7.3
CaO	10.2–11.5	3.6	2.9	12.8–14.7
Al_2O_3	10.5–12.5	14.0	15.5	5.8–6.4
SiO_2	42.2–43.6	52.9	52.9	44.5–48
Cl	4.5–5.4	0	0	3.5–3.9
F	2.4–3.2	0	0	3.7–4.6
H_2O	<1	15.2	19.1	< 1.5
Strongest reflections of the X-ray powder pattern: $d, \text{Å} - I$	9.65–100	6.523–100	6.857–58	3.528–29
	6.91–43	6.263–67	6.55–100	3.255–49
	6.59–97	3.062–91	4.787–96	3.080–100
	3.296–77	2.996–66	4.499–59	2.957–58
	3.118–70	2.955–63	3.065–86	2.904–66
	2.903–52	2.853–51	2.958–62	2.773–32
	2.819–53	2.763–60	2.767–62	1.860–27
Density, g/cm^3	2.49 (calc.)	2.18 (meas) 2.18 (calc)	2.16 (meas) 2.17 (calc)	2.56–2.60
Optical data				
α	1.537	1.488	1.496	1.528–1.532
β	1.543	1.490	1.498	1.529–1.533
γ	1.544	1.493	1.499	1.530–1.533
birefringence	0.007	0.005	0.003	< 0.003 (typically almost isotropic)
Optical sign, 2V	(–) 30°	(+) 30°	(–) 80°	(–) 80–90°
Sources	this paper	Chukanov <i>et al.</i> , 2012a; Rastsvetaeva <i>et al.</i> , 2012	Chukanov <i>et al.</i> , 2012b	Cannillo <i>et al.</i> (1969); Chukhrov (1992); Pekov <i>et al.</i> (2009)

*Unit cells of all minerals are given in the same setting with $b > a > c$.

Homogenization temperatures of inclusions are higher than 1000 °C in phenocrysts and 830–870 °C in groundmass kalsilite, nepheline and cuspidine (Stoppa *et al.*, 1997; Sharygin, 1999, 2001).

The heating experiments with melilite- and kalsilite-hosted inclusions have shown the following main events: melting of silicate glass occurred at 560–620 °C, carbonate globule began fusing at 600–650 °C, sulphides and westerveldite and one of colourless phases (umbrianite?) melt at 730–800 °C. In melilite-hosted inclusions, the colourless phases (cuspidine, kalsilite, nepheline) disappear at 850–900 °C, melting of phlogopite occurs at 950–1050 °C (Stoppa *et al.*, 1997; Sharygin, 1999, 2001). Summarizing these data, we conclude that crystallization of umbrianite may occur in the temperature range 620–800 °C.

In general, the evolution of the initial melilitolite melt had a phonolitic peralkaline character and was directed towards gradual increase of SiO₂, FeO, alkalis, light elements (B, Be, Li), Ba, S, F, Cl, possibly H₂O, and decrease of Al₂O₃, MgO, CaO (Sharygin, 1999, 2001). Crystallization of early minerals, separation of carbonatite liquid and possible CO₂ degassing seems to be responsible for the accumulation of trace elements and volatile components in residual peralkaline melts with (K + Na)/Al > 5. These factors stimulated the decrease of solidus temperature of the melt (down to 500–600 °C) and resulted in formation of specific phases (umbrianite, westerveldite, bartonite-chlorobartonite, bario-oligite, bafertisite, *etc.*) during the latest stage.

It should be mentioned that delhayelite, an analogue of umbrianite in the rhodesite series, also occurs in peralkaline volcanic and intrusive rocks only (Dorfman, 1958; Sahama & Hytönen, 1959; Dawson & Hill, 1998; Dawson, 1998; Sokolova *et al.*, 2005; Pekov *et al.*, 2011; Andersen *et al.*, 2012; Sharygin *et al.*, 2012; Zaitsev *et al.*, 2012). Chemical composition of residual glasses (melt inclusions, groundmass) in delhayelite-bearing volcanic rocks has shown that they are very highly alkaline to hyperagpaitic, with the (K + Na)/Al ratio ranging from 2 to 16 (Dawson & Hill, 1998; Andersen *et al.*, 2012; Sharygin *et al.*, 2012; Zaitsev *et al.*, 2012).

10. Concluding remarks

Umbrianite is a new member of the günterblässite group, a novel group of triple-layer silicates. The assumed alteration sequence umbrianite → Ba-rich phases → (günterblässite, hillesheimite) is very similar to that found in the rhodesite mero-pleisotype series (delhayelite → fivegite → hydrodelhayelite, Pekov *et al.*, 2009, 2011). From the structural point of view, umbrianite and Ba-rich phases are counterparts of günterblässite and hillesheimite in the (Si,Al)-ordering of tetrahedral blocks.

Acknowledgements: The first author thanks to L.N. Pospelova, E.N. Nigmatulina, N.S. Karmanov, A.T. Titov and S.Z. Smirnov for help in microprobe

analysis, scanning microscopy and Raman spectroscopy at the IGM, Novosibirsk. M.P. Mazurov (IGM) helped with measurement of the micro-indentation hardness. We are grateful to R. Wirth (GFZ, Potsdam) for HRTEM data of hydrated phases from the Pian di Celle and Sadiman volcanoes and S.G. Simak and Ye.V. Potapov (YBIPT, Yaroslavl) for SIMS analyses of umbrianite and delhayelite. X-ray powder diffraction measurements have been performed in the X-ray Diffraction Resource Centre of St. Petersburg State University. The manuscript was improved through comments and suggestions by editor S.V. Krivovichev and two anonymous reviewers. This work was supported by the Russian Foundation for Basic Research (grants 11-05-00875, 11-05-12001-ofi-m-2011 and 12-05-00250) and the Foundation of the President of the Russian Federation (grant NSh-2883.2012.5).

References

- Ageeva, O.A. (2002): Typomorphism of accessory minerals and evolution of mineral formation in rocks of ristschorrite complex (Khibiny Massif). PhD thesis, Moscow, MSU, 187 p. (in Russian).
- Alfors, J.T., Stinson, M.C., Matthews, R.A., Pabst, A. (1965): Seven new barium minerals from eastern Fresno County, California. *Am. Mineral.*, **50**, 314–340.
- Andersen, T., Elburg, M., Erambert, M. (2012): Petrology of combeite- and götzenite-bearing nephelinite at Nyiragongo, Virunga Volcanic Province in the East African Rift. *Lithos*, **152**, 105–121.
- Bellezza, M., Merlino, S., Perchiazzi, N. (2004): Chemical and structural study of the Zr,Ti-disilicates in the venanzite from Pian di Celle, Umbria, Italy. *Eur. J. Mineral.*, **16**, 957–969.
- Berger, J., Ennih, N., Mercier, J.-C.C., Liégeois, J.-P., Demaiffe, D. (2009): The role of fractional crystallization and late-stage peralkaline melt segregation in the mineralogical evolution of Cenozoic nephelinites/phonolites from Saghro (SE Morocco). *Mineral. Mag.*, **73**, 59–82.
- Cadoni, M. & Ferraris, G. (2009): Two new members of the rhodesite mero-pleisotype series close to delhayelite and hydrodelhayelite: synthesis and crystal structure. *Eur. J. Mineral.*, **21**, 485–493.
- Cannillo, E., Rossi, G., Ungaretti, L. (1969): The crystal structure of delhayelite. *Rend. Soc. Ital. Mineral. Petrol.*, **26**, 63–75.
- Chukanov, N.V., Rastsvetaeva, R.K., Aksenov, S.M., Pekov, I.V., Britvin, S.N., Belakovskiy, D.I., Schüller, W., Ternes, B. (2012a): Günterblässite, (K,Ca)_{3–x}Fe[(Si,Al)₁₃O₂₅(OH, O)₄] · 7H₂O, a new mineral, the first phyllosilicate with triple tetrahedral layer. *Geol. Ore Deposits*, **54**, 656–662.
- Chukanov, N.V., Zubkova, N.V., Pekov, I.V., Belakovskiy, D.I., Schüller, W., Ternes, B., Blaß, G., Pushcharovsky, D.Y. (2012b): Hillesheimite, (K,Ca,□)₂(Mg,Fe,Ca,□)₂[(Si,Al)₁₃O₂₃(OH)₆](OH)·8H₂O, a new phyllosilicate mineral of the günterblässite group. *Zapiski Rossiiskogo Mineralogicheskogo Obshchestva*, **141** (3), 29–39 (in Russian). English translation: *Geol. Ore Deposits*, **55**, in press.

- Chukhrov, F.V. (ed (1992): *Minerals. Vol. IV, Part 2. Phyllosilicates with Complex Tetrahedral Radicals*. Nauka Publishing, Moscow, 661 p. (in Russian).
- Cundari, A. & Ferguson, A.K. (1994): Appraisal of the new occurrence of götzenite_{ss}, khibinskite and apophyllite in kalsilite-bearing lavas from San Venanzo and Cupaello (Umbria), Italy. *Lithos*, **31**, 155–161.
- Dawson, J.B. (1998): Peralkaline nephelinite–natrocarbonatite relationships at Oldoinyo Lengai, Tanzania. *J. Petrol.*, **39**, 2077–2094.
- Dawson, J.B., & Hill, P.G. (1998): Mineral chemistry of a peralkaline combeite lamprophyllite nephelinite from Oldoinyo Lengai, Tanzania. *Mineral. Mag.*, **62**, 179–196.
- Dorfman, M.D. (1958): New data on mineralogy of Yukspor in the Khibiny Tundras. in “Problems of Geology and Mineralogy of the Kola Peninsula”, Moscow, PH AN SSSR, **1**, 146–150 (in Russian).
- Dorfman, M.D. & Chiragov, M.I. (1979): Hydrodelhayelite, a product of hypergene alteration of delhayelite. *New Data on Minerals*, **28**, 172–175 (in Russian).
- Hesse, K.-F., Liebau, F., Merlino, S. (1992): Crystal structure of rhodesite, $\text{HK}_{1-x}\text{Na}_{x+2y}\text{Ca}_{2-y}\{\text{IB},3,2^2_\infty\}[\text{Si}_8\text{O}_{19}]\cdot(6-z)\text{H}_2\text{O}$, from three localities and its relations to other silicates with dreier double layers. *Z. Kristallogr.*, **199**, 25–48.
- Jochum, K.P., Dingwell, D.B., Rocholl, A., Stoll, B., Hofmann, A.W., Becker, S., Besmehn, A., Bessette, D., Dietze, H.-J., Dulski, P., Erzinger, J., Hellebrand, E., Hoppe, P., Horn, I., Janssens, K., Jenner, G., Klein, M., McDonough, W.F., Maetz, M., Mezger, K., Munker, C., Nikogosian, I.K., Pickhart, C., Raczek, I., Rhede, D., Seufert, H.M., Simakin, S.G., Sobolev, A.V., Spettel, A.V., Straub, S., Vincze, L., Wallianos, A., Weckwerth, G., Weyer, S., Wolf, D., Zimmer, M. (2000): The preparation and preliminary characterisation of eight geological MPI-DING reference glasses for in-situ microanalysis. *Geostandard Newslett.*, **24**, 87–133.
- Lavecchia, G. & Boncio, P. (2000): Tectonic setting of the carbonatite-melilitite association of Italy. *Mineral. Mag.*, **64**, 583–592.
- Panina, L.I., Stoppa, F., Usol'tseva, L.M. (2003): Genesis of melilitite rocks of Pian di Celle volcano, Umbrian kamafugite province, Italy: evidence from melt inclusions in minerals. *Petrology*, **11**, 365–382.
- Peacor, D.R., Dunn, P.J., Simmons, W.B., Tillmanns, E., Fischer, R.X. (1984): Willhendersonite, a new zeolite isostructural with chabazite. *Am. Mineral.*, **69**, 186–189.
- Pekov, I.V., Zubkova, N.V., Chukanov, N.V., Sharygin, V.V., Pushcharovsky, D.Y. (2009): Crystal chemistry of delhayelite and hydrodelhayelite. *Dokl. Earth Sci.*, **428**, 1261–1211.
- Pekov, I.V., Zubkova, N.V., Filinchuk, Ya.E., Chukanov, N.V., Zadov, A.E., Pushcharovsky, D.Y., Gobechiya, E.R. (2010): Shlykovite $\text{KCa}[\text{Si}_4\text{O}_9(\text{OH})]\cdot 3\text{H}_2\text{O}$ and cryptophyllite $\text{K}_2\text{Ca}[\text{Si}_4\text{O}_{10}]\cdot 5\text{H}_2\text{O}$, new mineral species from the Khibiny alkaline pluton, Kola peninsula, Russia. *Geol. Ore Deposits*, **52**, 767–777.
- Pekov, I.V., Zubkova, N.V., Chukanov, N.V., Zadov, A.E., Pushcharovsky, D.Y. (2011): Fivegite, $\text{K}_4\text{Ca}_2[\text{AlSi}_7\text{O}_{17}(\text{O}_{2x}\text{OH}_x)] [(\text{H}_2\text{O})_{2-x}\text{OH}_x]\text{Cl}$: a new mineral from the Khibiny alkaline complex, Kola Peninsula, Russia. *Geol. Ore Deposits*, **53**(7), 591–603.
- Ragimov, K.G., Chiragov, M.I., Mamedov, K.S., Dorfman, M.D. (1980): Crystal structure of hydrodelhayelite, $\text{KH}_2\text{Ca}_2(\text{Si},\text{Al})_8\text{O}_{19}\cdot 6\text{H}_2\text{O}$. *Dokl. Akad. Nauk Azerb. SSR*, **36**(12), 49–51 (in Russian).
- Rastsvetaeva, R.K., Aksenov, S.M., Chukanov, N.V. (2012): Crystal structure of günterblässite, a new mineral with a triple tetrahedral layer. *Dokl. Chem.*, **442**(2), 57–62.
- Sahama, T.G. & Hytönen, K. (1959): Delhayelite, a new silicate from the Belgian Congo. *Mineral. Mag.*, **32**, 6–9.
- Sharygin, V.V. (1999): Boron-rich glasses in melilitolite from Pian di Celle, Umbria, Italy. *Terra Nostra*, **6**, 268–270.
- (2001): Silicate-carbonate liquid immiscibility in melt inclusions from melilitolite minerals: the Pian di Celle volcano (Umbria, Italy). *Memórias*, **7**, 399–402.
- (2002): Delhayelite from the Khibiny massif pegmatites and delhayelite-like mineral from melilitolites of the Pian di Celle volcano (San-Venanzo, Italy). in Abstracts of 19th conference “Geochemistry of magmatic rocks”, School “Alkaline magmatism of the Earth”, Moscow, 105–105 (in Russian).
- (2012): Magnesian kirschsteinite in melilitolites of the Pian di Celle volcano, Umbria, Italy. in Abstracts of 29th International conference “Ore potential of alkaline, kimberlite and carbonatite magmatism”, School “Alkaline magmatism of the Earth”, Sudak-Moscow, 154–155. <http://alkaline.web.ru/2012/abstracts/SharyginV.htm>
- Sharygin, V.V., Stoppa, F., Kolesov, B.A. (1996a): Cuspidine from melilitolites of San Venanzo, Italy. *Dokl. Akad. Nauk.*, **348**, 800–804.
- Sharygin, V.V., Stoppa, F., Kolesov, B.A. (1996b): Zr-Ti-bearing disilicates from Pian di Celle volcano (Umbria, Italy). *Eur. J. Mineral.*, **8**, 1199–1212.
- Sharygin, V.V., Kamenetsky, V.S., Zaitsev, A.N., Kamenetsky, M.B. (2012): Silicate-natrocarbonatite liquid immiscibility in 1917 eruption combeite-wollastonite nephelinite, Oldoinyo Lengai volcano, Tanzania: melt inclusion study. *Lithos*, **152**, 23–39.
- Sheldrick, G.M. (2008): A short history of SHELX. *Acta Crystallogr.*, **A 64**, 112–122.
- Sokolova, M.N., Smol'yaninova, N.N., Golovanova, T.I., Chukanov, N.V., Dmitrieva, M.T. (2005): Delhayelite crystals from ristschorrites of the Rasvumchorr Plateau (Khibiny Massif). *New Data on Minerals*, **40**, 115–118.
- Stoppa, F. (1995): The San Venanzo maar and tuff-ring, Umbria, Italy: eruptive behaviour of a carbonatite-melilitite volcano. *Bull. Volcanol.*, **57**, 563–567.
- Stoppa, F. & Cundari, A. (1998): Origin and multiple crystallization of the kamafugite-carbonatite association: the San Venanzo – Pian di Celle occurrence (Umbria, Italy). *Mineral. Mag.*, **62**, 273–289.
- Stoppa, F. & Woolley, A.R. (1997): The Italian carbonatites: field occurrence, petrology and regional significance. *Mineral. Petrol.*, **59**, 43–67.
- Stoppa, F., Sharygin, V.V., Cundari, A. (1997): New mineral data from the kamafugite-carbonatite association: the melilitolite from Pian di Celle, Italy. *Mineral. Petrol.*, **61**, 27–45.
- Zaitsev, A.N., Marks, M.A.W., Wenzel, T., Spratt, J., Sharygin, V.V., Strekopytov, S., Markl, G. (2012): Mineralogy, geochemistry and petrology of the phonolitic to nephelinitic Sadiman volcano, Crater Highlands, Tanzania. *Lithos*, **152**, 66–83.
- Zanon, V. (2005): Geology and volcanology of San Venanzo volcanic field (Umbria, Central Italy). *Geol. Mag.*, **142**(6), 683–698.
- Zubkova, N.V., Filinchuk, Y.E., Pekov, I.V., Pushcharovsky, D.Y., Gobechiya, E.R. (2010): Crystal structures of shlykovite and cryptophyllite: comparative crystal chemistry of phyllosilicate minerals of the mountainite family. *Eur. J. Mineral.*, **22**, 547–555.

Received 27 October 2012

Modified version received 31 January 2013

Accepted 18 March 2013